photoreceptor, the conductor Fermi level, the barrier height, and the position of the semiconductor conduction band edges, (2) the ballistic mean free path of electrons, and (3) the physical and electronic coupling of the chromophore to the conductor for high absorbance and high electron transfer efficiency. The devices studied here represent only one of several different configurations of photovoltaics taking advantage of ballistic electron transport and internal electron emission in a photovoltaic device. For example, modifications of the structure to utilize hot hole injection (rather than hot electrons) in a p-type junction[9] would allow use of hole conducting polymers instead of inorganic semiconductors.

The IPCE and overall energy efficiency are limited by low dye coverage (8×10^{14} molecules cm^{-2}) and the resulting low photon absorption. Significant increases are expected with improved optical design (reduced surface reflection), decreased metal thickness, increased dye loading, and an engineered surface morphology with significantly higher surface area structured such that multiple passes through a dye-covered surface are possible for each photon. Although the ultimate efficiency of an optimized device based on the concept presented here is approximately the same as an ideal conventional semiconductor cell, there appear to be practical and economic advantages in terms of the wide choice of inexpensive, durable, and readily synthesized device materials that may be utilized. □

Methods

Device fabrication

Devices were fabricated on titanium foil substrates (Alfa Aesar), which served as ohmic back contacts. A 250-nm layer of titanium (99.9999%) was evaporated under vacuum onto the foil following cleaning and polishing (using 10 μm grit). A 200-nm layer of TiO_2 was grown on the substrate by thermal oxidation at 500 °C. The polycrystalline TiO_2 is predominately rutile phase, with oxygen vacancies giving rise to n-type doping. Au films were electrodeposited onto the TiO_2 from a solution containing 0.2 M KCN and 0.1 M AuCN at pH 14. The TiO_2 served as the working electrode, with a Pt wire counter electrode. A 100-ms galvanostatic pulse at -200 mA cm^{-2} was used to nucleate Au uniformly on the surface, followed by a periodic galvanostatic pulse train of 5 ms at $+0.2$ mA cm^{-2} and 5 ms at -1.7 mA cm^{-2} for 10 s to form a film ~10–50 nm thick. Photoactive merbromin (2,7-dibromo-5-(hydroxymercurio)fluorescein disodium salt, 5 mM in water) was adsorbed onto the surface by immersion at room temperature for 10–12 h, followed by rinsing in water.

Characterization

Current–voltage (I–V) curves were measured using a voltage ramp rate of 0.05 V s^{-1} in the dark and under illumination from a 250-W tungsten lamp (Oriel, 6129), with intensity measured using a radiometer (IL1700, International Light). The fill factor was calculated at 1,000 W m^{-2} by dividing the maximum product of current and voltage from the illuminated I–V curve by the product of open-circuit voltage and short-circuit current at the same illumination. The spectral response was determined using a 150-W Xe lamp and monochromator (Oriel 7240). IPCE was calculated from the current density under short-circuit conditions and the photon flux as measured by the radiometer. The optical absorbance (and absorption efficiency, $\eta_\gamma(\varepsilon_\gamma)$) of the dye on the device surface and dye photon absorption was determined from the transmission and reflectance of a device fabricated on a transparent substrate before and after application of the dye, using an integrating sphere (LabSphere) and fibre-optic coupled monochromator (Ocean Optics). Free-solution dye absorbance was measured with an optical spectrometer (UV-1610, Shimadzu). Dye loading was determined by detaching the dye from the activated device surface in 1 mM NaOH solution, and determining the amount removed from the difference in optical absorbance at 511 nm of the NaOH solution.

Received 17 July; accepted 18 November 2002; doi:10.1038/nature01316.

1. Chapin, D. M., Fuller, C. S. & Pearson, G. L. A new silicon p-n junction photocell for converting solar radiation into electrical power. *J. Appl. Phys.* **25,** 676–677 (1954).
2. Archer, M. D. & Hill, R. (eds) *Clean Electricity from Photovoltaics* (Series on Photoconversion of Solar Energy, **Vol. 1,** Imperial College Press, London, 2001).
3. Goetzberger, A. & Hebling, C. Photovoltaic materials, past, present, future. *Sol. Energy Mater. Sol. Cells* **62,** 1–19 (2000).
4. Seah, M. P. & Dench, W. A. Quantitative electron spectroscopy of surfaces: a standard data base for electron inelastic mean free paths in solids. *Surf. Interf. Anal.* **1,** 2–11 (1979).
5. Frese, K. W. & Chen, C. Theoretical models of hot carrier effects at metal-semiconductor electrodes. *J. Electrochem. Soc.* **139,** 3234–3249 (1992).
6. Grätzel, M. Photoelectrochemical cells. *Nature* **414,** 338–344 (2001).
7. Green, M. A., Emery, K., King, D. L., Igari, S. & Warta, W. Solar cell efficiency tables (version 17). *Prog. Photovolt. Res. Applic.* **9,** 49–56 (2001).
8. Sze, S. M. *Physics of Semiconductor Devices* 2nd edn, Ch. 14 (Wiley & Sons, New York, 1981).
9. Nienhaus, H. *et al.* Electron-hole pair creation at Ag and Cu surfaces by adsorption of atomic hydrogen and deuterium. *Phys. Rev. Lett.* **82,** 446–448 (1999).

Acknowledgements We thank M. White, A. Tavakkoly, A. Kochhar, N. Shigeoka, G. Stucky and W. Siripala for technical assistance and discussions. The project was supported by Adrena Inc. Financial support for J.T. was provided by the NSF-MRSEC funded Materials Research Laboratory (UCSB).

Competing interests statement The authors declare competing financial interests: details accompany the paper on *Nature*'s website (http://www.nature.com/nature).

Correspondence and requests for materials should be addressed to E.W.M. (e-mail: mcfar@engineering.ucsb.edu).

Hydrothermal recharge and discharge across 50 km guided by seamounts on a young ridge flank

A. T. Fisher*†, E. E. Davis‡, M. Hutnak*, V. Spiess§, L. Zühlsdorff§, A. Cherkaoui*, L. Christiansen‖, K. Edwards¶, R. Macdonald‡, H. Villinger§, M. J. Mottl#, C. G. Wheat☆ & K. Becker¶

** Earth Sciences Department, † Institute for Geophysics and Planetary Physics, University of California, Santa Cruz, California 95064, USA*
‡ Pacific Geoscience Center, Geological Survey of Canada, Sydney, British Columbia V8L 4B2, Canada
§ Earth Sciences Department, University of Bremen, Bremen D-28359, Germany
‖ Department of Earth and Planetary Sciences, Johns Hopkins University, Baltimore, Maryland 21218, USA
¶ Rosenstiel School of Marine and Atmospheric Science, University of Miami, Miami, Florida 33149, USA
 # School of Earth and Ocean Science and Technology, University of Hawaii, Honolulu, Hawaii 96822, USA
☆ Global Undersea Research Unit, University of Alaska, Fairbanks, Alaska 99775, USA

Hydrothermal circulation within the sea floor, through lithosphere older than one million years (Myr), is responsible for 30% of the energy released from plate cooling, and for 70% of the global heat flow anomaly (the difference between observed thermal output and that predicted by conductive cooling models)[1,2]. Hydrothermal fluids remove significant amounts of heat from the oceanic lithosphere for plates typically up to about 65 Myr old[3,4]. But in view of the relatively impermeable sediments that cover most ridge flanks[5], it has been difficult to explain how these fluids transport heat from the crust to the ocean. Here we present results of swath mapping, heat flow, geochemistry and seismic surveys from the young eastern flank of the Juan de Fuca ridge, which show that isolated basement outcrops penetrating through thick sediments guide hydrothermal discharge and recharge between sites separated by more than 50 km. Our analyses reveal distinct thermal patterns at the sea floor adjacent to recharging and discharging outcrops. We find that such a circulation through basement outcrops can be sustained in a setting of pressure differences and crustal properties as reported in independent observations and modelling studies.

Hydrothermal circulation on ridge flanks (crust older than 1 Myr) advects lithospheric heat from much of the sea floor, contributing to enormous fluxes of fluid, energy and solutes[1,6,7]. It is easy for fluid to enter and leave the crustal reservoir on most young sea floor, where sediment cover is incomplete and permeable basement rocks are widely exposed, but mechanisms by which fluids penetrate through thick and more continuous sediments have remained enigmatic[5]. The primary difficulty is that forces available to drive hydrothermal circulation on ridge flanks are modest[7–10], being limited mainly to the difference in fluid pressures below

columns of recharging (cool) and discharging (warm) fluid. Sediment permeabilities are typically so low that even a few tens of metres of sediment cover will reduce seepage to rates that are incapable of liberating significant quantities of lithospheric heat[7,8]. Even sites located below areas of relatively rapid sedimentation may lose a considerable fraction of their heat advectively[11], but it has not been shown previously how hydrothermal fluids move across the thick sediment layer at rates sufficiently rapid to efficiently cool the oceanic crust over vast areas.

Ocean Drilling Program (ODP) Leg 168 investigated ridge-flank hydrothermal processes along an 80-km transect of sites east of the Juan de Fuca ridge[12] (Fig. 1a). Sediment cover over basement in this area is almost continuous at distances >20 km from the active spreading centre because of proximity to North America, a source for turbidites during Pleistocene glacial maxima. Pore fluids collected from just above basement along this transect[12], and recovered from an overpressured hole at Site 1026 that penetrated a buried basement ridge below 250 m of sediment[13] (Fig. 1b), were analysed for composition and ^{14}C age[14]. There is a general progression in fluid evolution along the western part of the drilling transect, as reaction temperatures rise, and ^{14}C ages increase from 1.0 to 9.9 thousand years (kyr) (relative to present bottom water) at distances of 3.3 to 14.6 km from the point of sediment onlap, respectively (Fig. 1a). But fluids collected from Site 1026 at the eastern end of the transect have a ^{14}C age of only 4.3 kyr, indicating that these waters could not have recharged near the western end of the drilling transect.

Swath map coverage of the region is extensive (Fig. 1b), and there are no known outcrops between exposed basement close to the spreading centre and Site 1026 that could have permitted recharge of younger water. There are several basaltic outcrops near Site 1026 (Fig. 1b) that are known sites of hydrothermal discharge[15–17]. The Baby Bare outcrop has been surveyed by surface ship, submersible, and remotely operated vehicle, and numerous vent sites have been located[16,18]. Baby Bare heat output is 2–20 MW, and the discharge flux of hydrothermal fluid is 4–13 l s^{-1} (refs 16, 19). Although Baby Bare rises just 65 m above the surrounding sea floor (Fig. 1c), the basaltic edifice is substantial, rising 600 m above regional basement (Fig. 2a).

Co-located heat-flow and seismic measurements across Baby

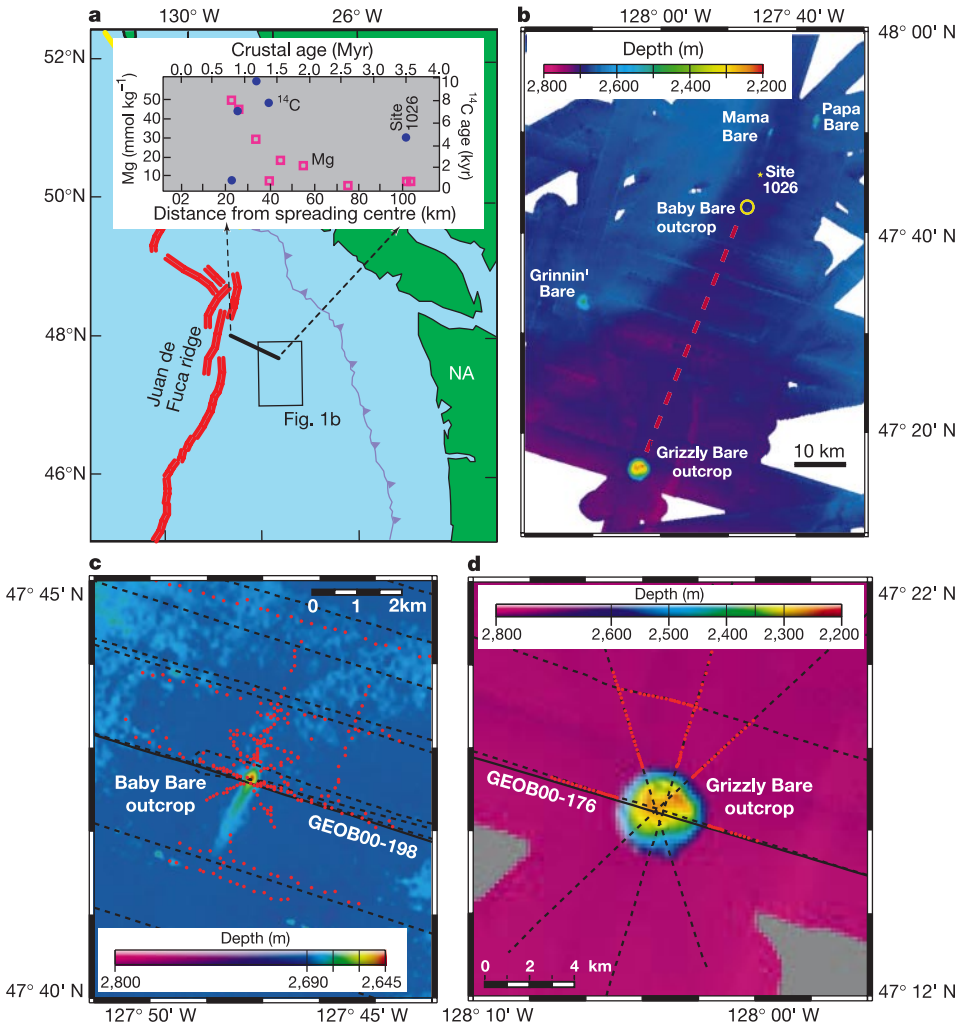

Figure 1 Maps of field area on the eastern flank of Juan de Fuca ridge, and selected geochemical data collected during ODP Leg 168[12]. **a**, Regional index map showing spreading ridges (red) and subduction zone (purple). NA, North America. Thick black line is Leg 168 transect. Inset, Mg concentrations and ^{14}C ages from upper basement pore fluids[14]. **b**, Swath map bathymetry showing locations of outcrops and ODP Site 1026 (star). Dashed red line indicates buried basement ridge, subparallel to spreading centre to the west, that runs between several outcrops and ODP Site 1026. **c**, Bathymetric detail around Baby Bare outcrop, showing locations of seismic profiles (black lines) and heat-flow measurements (red dots). Seismic profile GEOB00-198 (solid line) is shown in Fig. 2a. **d**, Bathymetric detail around Grizzly Bare outcrop. Symbols as in **c**. Seismic profile GEOB00-176 is shown in Fig. 2b.

Bare illustrate the local influence of fluid venting on the thermal state of the crust (Fig. 2a). Heat flow away from the outcrop is consistent with conductive cooling models for sea floor of this age, after correcting for sedimentation[20]. Heat flow is considerably greater within a few hundred metres of the outcrop, rising above $1\,W\,m^{-2}$. We have calculated isotherm depths near the outcrop by continuing sea-floor heat-flow values downwards to upper basement, on the basis of thermal and seismic data (Fig. 2a). Isotherms are generally subparallel to the sediment–basement interface until very close to the outcrop, with an upper basement temperature of about 65 °C, near that measured at Site 1026[13]. The rise in heat flow near the outcrop results from maintenance of nearly isothermal basement temperatures as sediment thins, indicating extremely vigorous local circulation.

Fluid seepage downwards through sediments near Baby Bare outcrop cannot recharge warm springs discharging on this feature. The youthful ^{14}C age of shallow basement fluids[14] would require a recharge velocity of at least $10\,cm\,yr^{-1}$, given typical sediment thickness. Geochemical analyses of pore fluids collected well away from basement highs in this area indicate diffusive and reactive conditions throughout the thick sediment layer, with no evidence for vertical advection[12,21]. These analyses are sensitive to fluid velocities $\geq 0.1\,mm\,yr^{-1}$, and thus an area of $1{,}500\,km^2$ around Baby Bare outcrop (a radial distance of 22 km) would be required to support discharge of $5\,l\,s^{-1}$. Even assuming a recharge velocity of $0.1\,mm\,yr^{-1}$, sediment properties[8,12] would require a much greater differential pressure than observed regionally[8,9,22] to draw bottom sea water downward through the sediment layer and into basement.

Sulphate compositions of Baby Bare vent fluids require recharge through basaltic outcrops[21]. There is no thermal or geochemical evidence for hydrothermal recharge through outcrops close to Baby Bare, but a consistent trend in the composition of basement pore fluids from south to north along the buried basement ridge below Baby Bare and Site 1026[23] indicates that recharge may occur to the south. We investigated the hydrogeology of the two closest outcrops south of Baby Bare. Heat-flow observations around the Grinnin' Bare outcrop, 35 km southwest of Baby Bare (Fig. 1b), are also indicative of fluid venting, but the Grizzly Bare outcrop, 52 km south-southwest of Baby Bare, hosts a contrasting thermal regime

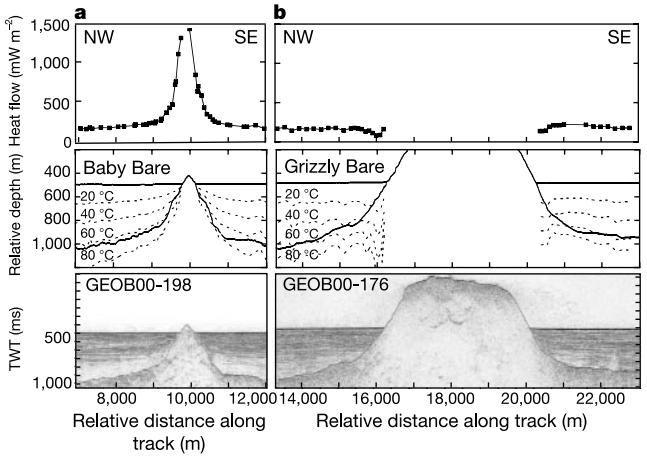

Figure 2 Heat-flow values, isotherms and seismic profiles across the Baby Bare and Grizzly Bare outcrops. Heat-flow values are those that are not on the outcrops and are within 100 m of the seismic lines. Typical sediment thickness away from the outcrops is about 500 m. Heat-flow values away from the outcrops are consistent with conductive cooling models for 3.5-Myr-old sea floor, after correcting for sedimentation[20], and upper basement temperatures are about 65 °C. **a**, Isotherms are subparallel to the sediment–basement interface in the vicinity of the Baby Bare outcrop, rising with basement abruptly near the outcrop. Isotherm locations are approximate, being based on the assumption of locally conductive conditions. **b**, Heat flow decreases near the edge of Grizzly Bare outcrop, and basement temperatures remain depressed out to a distance of several kilometres from the area of basement exposure. Local variations in heat flow—for example, the single elevated value adjacent to the northwest side of Grizzly Bare outcrop—are likely to result from irregularities in aquifer geometry and properties, and are most common where sediment cover is thin.

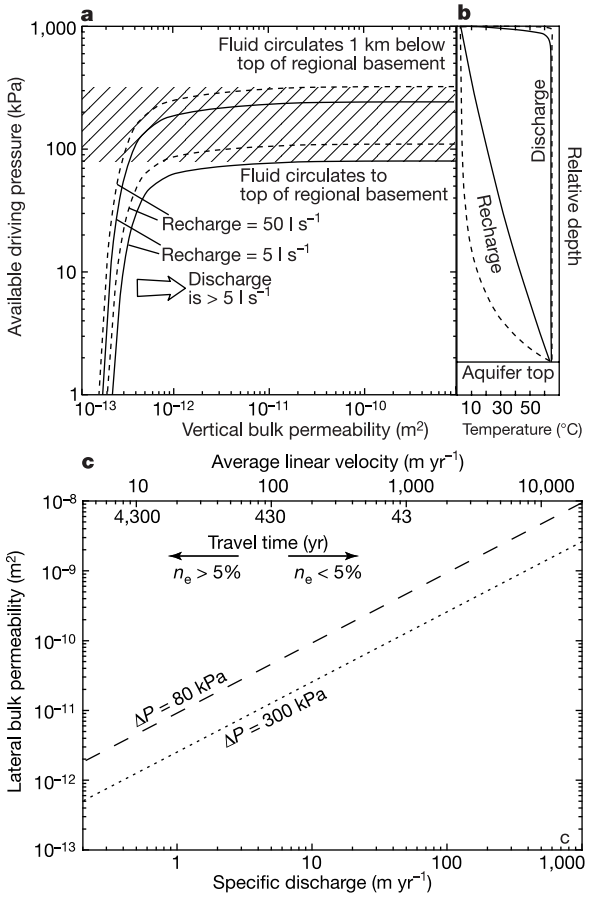

Figure 3 Calculated pressures available to drive large-scale lateral fluid flow, thermal profiles within outcrops, and lateral bulk permeabilities within basement between outcrops. **a**, Pressures available to drive large-scale lateral fluid flow within basement between Grizzly Bare (recharge) and Baby Bare (discharge) outcrops, based on the difference between pressures at the base of recharging and discharging columns of fluid. Calculations were completed for discharge of $5\,l\,s^{-1}$, and for recharge of $5\,l\,s^{-1}$ (solid line) and $50\,l\,s^{-1}$ (dashed line). The lower values in each case indicate results for fluid circulation to the top of regional basement, and the higher values show results for flow at a depth of 1 km below top of regional basement. Vertical permeabilities $<10^{-12}\,m^2$ would result in considerable energy being lost during ascent and descent, leaving less differential pressure to drive lateral flow at depth. Shaded band indicates range of driving pressures based on vertical permeability $>10^{-12}\,m^2$. Higher discharge values[19] would move the curves to the right, as indicated by the arrow, but would not change the pressure available to drive large-scale, lateral flow. **b**, Vertical thermal profiles at recharge and discharge sites were calculated using a one-dimensional model of heat and fluid flow[24], and volume fluxes of $5\,l\,s^{-1}$ (solid line) or $50\,l\,s^{-1}$ (dashed line). The calculated discharge profiles are more isothermal than the recharge profiles because the fluid is assumed to pass through a much smaller cross-sectional area at Baby Bare outcrop than at Grizzly Bare outcrop. **c**, Lateral bulk permeability required between the outcrops as a function of volume flow/area. Travel times and average linear velocities shown on upper axis are for an effective porosity, n_e, of 5%; higher or lower values would shift the upper axis as indicated with the arrows. The actual fluid travel time between outcrops cannot be greater than that the ^{14}C age of 4.3 kyr (ref. 14), but considerably shorter times are indicated once dispersive loss during flow is considered[25–27].

(Figs 1 and 2b). Heat flow away from Grizzly Bare is consistent with crustal age, but values drop abruptly by 50% adjacent to the outcrop. Isotherms within uppermost basement around Grizzly Bare are suppressed relative to those at Baby Bare out to several kilometres from the edge of basement exposure (Fig. 2b). These observations indicate that recharge of cold sea water cools the basement rocks. On the basis of geochemical observations[14,23] and a lack of other recharge or discharge sites between the two outcrops, we infer that some of the water recharging Grizzly Bare flows north-northeast and vents at the Baby Bare outcrop 52 km away.

To test whether this hydrogeologic interpretation is reasonable, we quantify available forces and basement properties necessary to drive fluid flow at rates consistent with observations (Fig. 3). In the absence of recent volcanism[18], driving forces responsible for large-scale lateral flow on ridge flanks are limited to the difference in pressure between recharging (cool) and discharging (warm) columns of water[9], $\Delta P = g\int_0^z \Delta\rho(z)\mathrm{d}z$, where g is the acceleration due to gravity, $\Delta\rho(z)$ is the difference in fluid density, and z is the height of recharging and discharging water columns. We calculate the pressure difference using a one-dimensional model of coupled heat and fluid flow with fixed upper and lower boundary temperatures[24], 2 °C and 65 °C, respectively. We use a hydrothermal discharge flux of $5\,\mathrm{l\,s^{-1}}$ (ref. 16), and recharge fluxes of $5\,\mathrm{l\,s^{-1}}$ and $50\,\mathrm{l\,s^{-1}}$. The first case presumes that all recharge at Grizzly Bare circulates to Baby Bare, whereas the second case supposes that only 10% of recharge follows that path (the rest venting elsewhere). We subtract the energy lost during vertical flow, using Darcy's law and assuming that recharge and discharge are distributed evenly across the outcrop surfaces. We make these calculations for various depths into basement, and show results for two extreme cases: fluid flows laterally at the top of regional basement (600 m below the sea floor), and fluid flows laterally 1,000 m into regional basement (1,600 m below the sea floor).

If vertical permeability within the two outcrops were $\leq 10^{-13}\,\mathrm{m^2}$, all energy available to drive lateral flow would be lost during fluid descent and ascent (Fig. 3a). At vertical permeabilities $\geq 10^{-12}\,\mathrm{m^2}$, little energy is lost during fluid descent and ascent, and 80–300 kPa could be available to drive lateral flow between the outcrops (Fig. 3a). The ^{14}C age of basement water from Site 1026 (4.3 kyr; ref. 14), which is geochemically very similar to Baby Bare vent fluids[23], provides an upper limit for the travel time between Grizzly Bare and Baby Bare. Studies of groundwater age demonstrate that large corrections are needed to account for dispersive losses between layers hosting the most significant flow and the stagnant layers around them[25–27]. Particularly within heterogeneous, fractured aquifers, corrections of the order of 10 to 100 times or more are required. If the actual travel time between outcrops is 4.3 kyr (no dispersive loss), and the driving pressure is 80–300 kPa, lateral bulk permeability of $\geq 10^{-12}\,\mathrm{m^2}$ is required (Fig. 3c). If the dispersive correction is 100 times, then bulk permeability would need to be $10^{-10}\,\mathrm{m^2}$ and the travel time between outcrops would be only about 40 yr (Fig. 3c).

Permeability values in upper basement of $\geq 10^{-12}\,\mathrm{m^2}$ were determined by borehole measurements at Site 1026[13], and values $\geq 10^{-10}\,\mathrm{m^2}$ were estimated on the basis of analysis of formation tidal response and considerations of thermal homogeneity[10,22]. Thus there is sufficient basement permeability and a large enough driving force to allow water recharging at the Grizzly Bare outcrop to discharge at the Baby Bare outcrop, 52 km to the north-northwest. Bulk permeability may be enhanced in this direction (subparallel to the spreading axis to the west) by faults and fractures in the crust developed during and after crustal creation. Sea-floor heat-flow values away from outcrops in the study area do not indicate a significant regional heat-flow deficit, as observed on most young ridge flanks[3,4], so the fluid flux through upper basement must be relatively modest. This is probably a result of the thick and mostly continuous sediment cover that isolates much of the basement aquifer from easy communication with the overlying ocean.

Seamounts and other basement outcrops are common features on a global basis[28,29], and the processes documented by this study illustrate how hydrogeologic communication between the hydrothermal entry and exit points is possible over large distances. This explains how much of the sea floor, which is typified by a greater density of basement outcrops than found on the eastern Juan de Fuca ridge flank, can experience pervasive advective heat loss even while sealed locally below thick sediments. □

Received 4 September; accepted 26 November 2002; doi:10.1038/nature01352.

1. Elderfield, H. & Schultz, A. Mid-ocean ridge hydrothermal fluxes and the chemical composition of the ocean. *Annu. Rev. Earth Planet. Sci.* **24,** 191–224 (1996).
2. Sclater, J. G., Jaupart, C. & Galson, D. The heat flow through oceanic and continental crust and the heat loss of the earth. *Rev. Geophys. Space Phys.* **18,** 269–311 (1980).
3. Parsons, B. & Sclater, J. G. An analysis of the variation of ocean floor bathymetry and heat flow with age. *J. Geophys. Res.* **82,** 803–829 (1977).
4. Stein, C. & Stein, S. A model for the global variation in oceanic depth and heat flow with lithospheric age. *Nature* **359,** 123–129 (1992).
5. Jacobson, R. S. Impact of crustal evolution on changes of the seismic properties of the uppermost oceanic crust. *Rev. Geophys.* **30,** 23–42 (1992).
6. Williams, D. L. & Von Herzen, R. P. Heat loss from the earth: new estimate. *Geology* **2,** 327–328 (1974).
7. Mottl, M. J. & Wheat, C. G. Hydrothermal circulation through mid-ocean ridge flanks: fluxes of heat and magnesium. *Geochim. Cosmochim. Acta* **58,** 2225–2237 (1994).
8. Giambalvo, E., Fisher, A. T., Darty, L., Martin, J. T. & Lowell, R. P. Origin of elevated sediment permeability in a hydrothermal seepage zone, eastern flank of Juan de Fuca Ridge, and implications for transport of fluid and heat. *J. Geophys. Res.* **105,** 913–928 (2000).
9. Fisher, A. & Becker, K. Channelized fluid flow in oceanic crust reconciles heat-flow and permeability data. *Nature* **403,** 71–74 (2000).
10. Davis, E. E. & Becker, K. Observations of natural-state fluid pressures and temperatures in young oceanic crust and inferences regarding hydrothermal circulation. *Earth. Planet. Sci. Lett.* **204,** 231–248 (2002).
11. Baker, P., Stout, P., Kastner, M. & Elderfield, H. Large-scale lateral advection of seawater through oceanic crust in the central equatorial Pacific. *Earth. Planet. Sci. Lett.* **105,** 522–533 (1991).
12. Davis, E. E., Fisher, A. T., Firth, J. *Proc. ODP Init. Rep.* Leg 168 (1997).
13. Fisher, A. T., Becker, K. & Davis, E. E. The permeability of young oceanic crust east of Juan de Fuca Ridge determined using borehole thermal measurements. *Geophys. Res. Lett.* **24,** 1311–1314 (1997).
14. Elderfield, H., Wheat, C. G., Mottl, M. J., Monnin, C. & Spiro, B. Fluid and geochemical transport through oceanic crust: a transect across the eastern flank of the Juan de Fuca Ridge. *Earth. Planet. Sci. Lett.* **172,** 151–165 (1999).
15. Davis, E. E. *et al.* FlankFlux: an experiment to study the nature of hydrothermal circulation in young oceanic crust. *Can. J. Earth Sci.* **29,** 925–952 (1992).
16. Mottl, M. J. *et al.* Warm springs discovered on 3.5 Ma oceanic crust, eastern flank of the Juan de Fuca Ridge. *Geology* **26,** 51–54 (1998).
17. Wheat, C. G. & Mottl, M. Composition of pore and spring waters from Baby Bare: global implications of geochemical fluxes from a ridge flank hydrothermal system. *Geochim. Cosmochim. Acta* **64,** 629–642 (2000).
18. Becker, N. C., Wheat, C. G., Mottl, M. J., Karsten, J. & Davis, E. E. A geological and geophysical investigation of Baby Bare, locus of a ridge flank hydrothermal system in the Cascadia Basin. *J. Geophys. Res.* **105,** 23557–23568 (2000).
19. Thomson, R. E., Davis, E. E. & Burd, B. J. Hydrothermal venting and geothermal heating in Cascadia Basin. *J. Geophys. Res.* **100,** 6121–6141 (1995).
20. Davis, E. E. *et al.* Regional heat-flow variations across the sedimented Juan de Fuca Ridge eastern flank: constraints on lithospheric cooling and lateral hydrothermal heat transport. *J. Geophys. Res.* **104,** 17675–17688 (1999).
21. Wheat, C. G. & Mottl, M. J. Hydrothermal circulation, Juan de Fuca Ridge eastern flank: factors controlling basement water composition. *J. Geophys. Res.* **99,** 3067–3080 (1994).
22. Davis, E. E., Wang, K., Becker, K. & Thompson, R. E. Formation-scale hydraulic and mechanical properties of oceanic crust inferred from pore-pressure response to periodic seafloor loading. *J. Geophys. Res.* **105,** 13423–13435 (2000).
23. Wheat, C. G., Elderfield, H., Mottl, M. J. & Monnin, C. Chemical composition of basement fluids within an oceanic ridge flank: implications for along-strike and across-strike hydrothermal circulation. *J. Geophys. Res.* **105,** 13437–13447 (2000).
24. Bredehoeft, J. D. & Papadopulos, I. S. Rates of vertical groundwater movement estimated from the earth's thermal profile. *Wat. Resour. Res.* **1,** 325–328 (1965).
25. Sanford, W. E. Correcting for diffusion in carbon-14 dating of ground water. *Ground Wat.* **35,** 357–361 (1997).
26. Bethke, C. M. & Johnson, T. M. Paradox of groundwater age. *Geology* **30,** 107–110 (2002).
27. Shapiro, A. M. Effective matrix diffusion in kilometer-scale transport in fractured rock. *Wat. Resour. Res.* **37,** 507–522 (2001).
28. Wessel, P. Global distribution of seamounts inferred from gridded Geosat/ERS-1 altimetry. *J. Geophys. Res.* **106,** 19431–19442 (2001).
29. Villinger, H., Grevemeyer, I., Kaul, N., Hauschild, J. & Pfender, M. Hydrothermal heat flux through aged oceanic crust: where does the heat escape? *Earth. Planet. Sci. Lett.* **202,** 159–170 (2002).

Acknowledgements This work was supported by the NSF, LANL/CULAR, and IGPP at UCSC.

Competing interests statement The authors declare that they have no competing financial interests.

Correspondence and requests for materials should be addressed to A.F. (e-mail: afisher@es.ucsc.edu).